

Radial Acceleration Relation of HI-rich Low Surface Brightness Galaxies

Zichen Hua^{1,2}, Yu Rong^{1,2*}, Huijie Hu^{3,4}

¹Department of Astronomy, University of Science and Technology of China, Hefei 230026, China

²School of Astronomy and Space Sciences, University of Science and Technology of China, Hefei 230026, China

³University of Chinese Academy of Sciences, Beijing 100049, China

⁴National Astronomical Observatories, Chinese Academy of Sciences, Beijing 100012, China

arXiv:2403.16754v1 [astro-ph.GA] 25 Mar 2024

Accepted XXX. Received YYY; in original form ZZZ

ABSTRACT

We investigate the radial acceleration relation (RAR) in low surface brightness galaxies selected from the Arecibo Legacy Fast ALFA survey. We find that the dynamical acceleration g_{obs} and baryonic gravitational acceleration g_{bar} of the HI-rich low surface brightness galaxies still follow the universal RAR of typical late-type galaxies. The universal RAR signifies a consistent correlation between the distribution of baryonic matter and dark matter across galaxies with diverse morphologies and properties. Our findings suggest that the matter distributions in low surface brightness galaxies may indeed resemble that of general late-type galaxies. This implies that low surface brightness galaxies may not originate from dark matter halos with lower densities; instead, they may originate from the dark matter halos with high spins or form through feedback processes.

Key words: galaxies: kinematics and dynamics – galaxies: formation – galaxies: evolution

1 INTRODUCTION

Low surface brightness galaxies (LSBGs) constitute a special population of galaxies with central surface brightness at least one magnitude fainter than that of the sky background (i.e., B -band surface brightness $\geq 22.5 \text{ mag} \cdot \text{arcsec}^{-2}$; Impey & Bothun 1997; Bothun et al. 1997). LSBGs have been observed to exhibit higher HI fractions (Du et al. 2015; He et al. 2020), lower star formation rates (Wyder et al. 2009; Rong et al. 2020b), and low metallicities (Kuzio de Naray et al. 2004). Also, they tend to appear in low-density environments (Pérez-Montañó & Cervantes Sodi 2019; Mo et al. 1994).

The distribution of dark matter and baryonic matter in LSBGs exhibits a high degree of diversity. Regarding the mass ratio of baryonic matter to dark matter, many studies have shown that the dynamics of LSBGs are dominated by dark matter (e.g. de Blok & McGaugh 1997; Mowla et al. 2017), while a particular LSBG population, ultra-diffuse galaxies (UDGs), may be dark matter deficient (e.g. van Dokkum et al. 2018; Mancera Piña et al. 2019). Similarly, investigations into the baryonic Tully-Fisher relation (BTFR, see McGaugh et al. 2000 and other sources) of LSBGs seem to yield conflict outcomes. For instance, Lelli et al. (2016b) find that the BTFR of galaxies do not correlate with the surface brightness of the galaxies; whereas Hu et al. (2023) find UDGs that deviate significantly from the BTFR of typical galaxies. The stellar mass-halo mass relation ($M_* - M_{\text{halo}}$) also presents a similar situation. While Prole et al. (2019) suggest that LSBGs form a continuous extension of typical dwarfs in the $M_* - M_{\text{halo}}$ diagram, others find that UDGs deviate significantly from the typical $M_* - M_{\text{halo}}$ relation (e.g., van Dokkum et al. 2018). This diversity in matter distribution among LSBGs may provide valuable insights into their varied formation and evolution

pathways. Therefore, understanding these differences is crucial for refining our current models of galaxy formation and evolution.

Studies suggest that the low-mass LSBGs may be failed L^* galaxies (van Dokkum et al. 2015a,b), or dwarf galaxies hosted in halos belonging to the high-end tail of the spin-distribution (Rong et al. 2017; Amorisco & Loeb 2016; Kim & Lee 2013). There are also studies suggesting that they were formed in low-density dark matter halos (Dekel & Silk 1986; McGaugh 1992; Mo et al. 1994). In addition, they may originate from early mergers (Wright et al. 2021) or stellar feedback processes (Chan et al. 2018) or tides (Rong et al. 2020a; Carleton et al. 2019) as well. As for high-mass LSBGs, their formation might due to mergers (Saburova et al. 2018; Zhu et al. 2023), two-stage process with external gas accretions (Saburova et al. 2021), or dynamical evolution originated from the bars (Noguchi 2001). However, current studies on the mass distributions in LSBGs have not achieved consensus. A complete scenario has not been drawn to restrict current formation models of LSBGs and understand the formation and evolution of LSBGs.

Recently, a series of studies (McGaugh et al. 2016; Lelli et al. 2017; Li et al. 2018; Richards et al. 2018; Rong et al. 2018; Chae et al. 2020) have discovered a radial acceleration relation (RAR), i.e., the acceleration g_{bar} produced by the baryonic mass and the acceleration g_{obs} produced by the dynamical mass at any radius in many types of galaxies are tightly correlated, which indicates a universally established correlation between the mass distributions of baryonic matter and dark matter in galaxies. Despite minor variations in specific details, standard Λ CDM models employing abundance matching procedures (e.g. Behroozi et al. 2013; Kravtsov et al. 2018), along with proper scaling relations, generally reproduce the universal RAR (Ludlow et al. 2017; Navarro et al. 2017; Keller & Wadsley 2017; Wheeler et al. 2019; Li et al. 2022). Consequently, investigating the RAR in LSBGs may shed light on whether LSBGs adhere to the

* Corresponding author; E-mail: rongyu@ustc.edu.cn

scaling relationships of typical galaxies. Besides, testing the RAR of LSBGs may also reveal information about their stellar feedback process (Grudić et al. 2020) and the relaxation process of their dark matter halos (Paranjape & Sheth 2021). By comparing the RAR of LSBGs to that of typical late-type galaxies, we can ascertain whether LSBGs exhibit similar distribution patterns of matter as general late-type galaxies, thus providing constraints on the formation mechanisms of LSBGs.

In this work, we will first introduce our sample selection in Section 2, and then describe our methods for calculating g_{bar} and g_{obs} in Section 3. We will then present our results in Section 4, and finally discuss the possible formation mechanism of LSBGs supported by our results in Section 5.

2 SAMPLE SELECTION

The Arecibo Legacy Fast ALFA survey (ALFALFA) is a wide-area blind HI survey aimed at searching for HI-bearing objects in the extragalactic neighbourhood. Haynes et al. (2011) matched the HI sources in the ALFALFA $\alpha.40$ catalogue with the optical counterparts in the Sloan Digital Sky Survey (SDSS) Data Release 7 (DR7) and obtained the ALFALFA-SDSS $\alpha.40$ cross-matched catalogue. From this catalogue, Du et al. (2015) and He et al. (2020) have selected a sample of LSBGs, which is treated as our parent sample.

From this parent sample, we first remove LSBGs with g -band apparent axis ratios $b/a > 0.72$, corresponding to the threshold of inclination angles of $i \lesssim 45^\circ$ (see equation (16)), because the spherical ones may introduce large uncertainties in the measurements of the rotation velocities. We then exclude LSBGs with low HI spectral signal-to-noise ratios $\text{SNR} < 10$, and visually remove LSBGs with suspicious HI spectra.

Due to the spatial resolution of ALFALFA being $3.8' \times 3.3'$ (Durbala et al. 2020), if a galaxy has neighbouring galaxies, its HI spectrum may be contaminated by the companions. To eliminate this possibility, we remove samples with neighbouring galaxies within the projected radii of $3.8'$ (i.e., approximately the beam size of Arecibo) and radial velocity differences of $\Delta v < 500\text{km/s}$. The redshift of LSBGs is assumed to be the central velocity of its HI spectrum, while the redshift of the neighbouring galaxies comes from the SpecObj and Photoz databases of SDSS. Finally, 207 LSBGs are left in our sample.

We also calculate the kurtosis coefficients, k_4 , of the HI spectra (Papastergis et al. 2016; El-Badry et al. 2018) for our sample galaxies, as

$$k_4 = M_4 / \sigma^4 - 3, \quad (1)$$

where M_4 and σ^2 are calculated as,

$$M_4 = \int_{\nu_{\min}}^{\nu_{\max}} (\nu - \bar{\nu})^4 F(\nu) d\nu / \int_{\nu_{\min}}^{\nu_{\max}} F(\nu) d\nu, \quad (2)$$

$$\sigma^2 = \int_{\nu_{\min}}^{\nu_{\max}} (\nu - \bar{\nu})^2 F(\nu) d\nu / \int_{\nu_{\min}}^{\nu_{\max}} F(\nu) d\nu. \quad (3)$$

In equations (2) and (3), ν and $F(\nu)$ represent the frequency and the flux density, respectively, and $\bar{\nu}$ is defined as,

$$\bar{\nu} = \int_{\nu_{\min}}^{\nu_{\max}} \nu F(\nu) d\nu / \int_{\nu_{\min}}^{\nu_{\max}} F(\nu) d\nu. \quad (4)$$

Here, ν_{\min} and ν_{\max} correspond to the minimal and maximum frequencies between which W_{20} (see Section 3 for the definition of W_{20}) is measured, respectively. The coefficient k_4 quantifies the ‘peakiness’ of a spectrum and thus can indicate whether a spectrum

is single-peaked or double-horned. The single-peaked galaxies may have kinematics strongly influenced by velocity dispersion (El-Badry et al. 2018), or HI disks that are not extended enough (Papastergis et al. 2016). As a consequence, their HI-widths might not represent their rotation velocities (McGaugh 2012; Verheijen 1997). Therefore, we perform a cut at the HI spectrum, $k_4 < -1$, in order to remove the single-peaked galaxies.

The final sample contains 127 high-quality LSBGs with double-horned HI lines, ensuring the most reliable results. For comparison, 207 high surface brightness galaxies (HSBGs, $\mu_{0B} < 22.5\text{ mag}$) with double-horned HI lines are also selected from our parent sample as the counterparts.

3 METHOD

We test the RAR by calculating the acceleration g_{bar} produced by baryonic matter and the dynamical acceleration g_{obs} in galaxies. g_{bar} is calculated as,

$$\nabla^2 \Phi = 4\pi G \rho, \quad (5)$$

$$g_{\text{bar}} = -\frac{\partial \Phi}{\partial R}, \quad (6)$$

where Φ is the gravitational potential, G is the gravitational constant, ρ is the density of baryonic matter, and R is the radius. The baryonic matter in galaxies is mainly composed of stars and gas. Our LSBGs mostly exhibit disk-dominated optical characteristics with a Sérsic index of $n \sim 1$ (Du et al. 2015; He et al. 2020). Gas is usually assumed to follow an exponential disk. Therefore, we model the stars and the gas separately according to the standard thin-disk distribution.

The surface density profile of the stellar disk can be written as,

$$\Sigma_*(R) = \frac{M_*}{2\pi R_{\text{d},*}^2} \exp\left(-\frac{R}{R_{\text{d},*}}\right), \quad (7)$$

where $R_{\text{d},*}$ is related to the effective radius R_{eff} in the g -band by a factor 1.678, i.e., $R_{\text{d},*} = R_{\text{eff}}/1.678$. The stellar mass M_* can be obtained with the galaxy luminosity in the W1-band (denoted as L_{W1}), from the Wide-field Infrared Survey Explorer, using the method proposed by McGaugh & Schombert (2015),

$$M_*/M_{\odot} = 0.45 L_{\text{W1}} / L_{\odot}, \quad (8)$$

Analogously, the surface density profile of the gas can be expressed as,

$$\Sigma_{\text{g}}(R) = \frac{M_{\text{g}}}{2\pi R_{\text{d},\text{g}}^2} \exp\left(-\frac{R}{R_{\text{d},\text{g}}}\right), \quad (9)$$

where M_{g} is the gas mass. Since the mass of molecular gas in a galaxy is low compared with the masses of HI and helium, we then neglect it (McGaugh 2012) and estimate M_{g} by adding up the mass of HI and helium,

$$M_{\text{g}} = 1.33 M_{\text{HI}}, \quad (10)$$

where M_{HI} is the HI mass. The value of $R_{\text{d},\text{g}}$ can be derived from the HI radius R_{HI} and M_{HI} , where R_{HI} is defined as the radius at which the HI density is $\Sigma_{\text{HI}}(R_{\text{HI}}) = 1 M_{\odot}\text{pc}^{-2}$ (Broeils & Rhee 1997). R_{HI} has been found to exhibit a tight correlation with M_{HI} (Wang et al. 2016), as

$$\log\left(\frac{2R_{\text{HI}}}{\text{kpc}}\right) = (0.506 \pm 0.003) \log\left(\frac{M_{\text{HI}}}{M_{\odot}}\right) - (3.293 \pm 0.009). \quad (11)$$

This correlation has been found to hold consistently across various

galaxy types, including UDGs and other LSBGs (Wang et al. 2016; Leisman et al. 2017; Gault et al. 2021).

Finally, equation (6) can be written as (Freeman 1970),

$$g_{\text{bar}} = f\left(\frac{R}{2R_{\text{d},*}}\right) \frac{GM_*}{R^2} + f\left(\frac{R}{2R_{\text{d},g}}\right) \frac{GM_{\text{g}}}{R^2}, \quad (12)$$

$$f(y) = 4y^3 [I_0(y)K_0(y) - I_1(y)K_1(y)], \quad (13)$$

where I_n , K_n are the modified Bessel functions of the first and second kind, respectively.

For the dynamical acceleration g_{obs} , we employ the following equation,

$$g_{\text{obs}} = \frac{v_{\text{rot}}^2}{R}, \quad (14)$$

where v_{rot} represents the rotation velocity of a galaxy. The rotation velocity is usually estimated using the 20% peak widths of the HI spectra (W_{20}) in the previous studies (e.g. Guo et al. 2020; Hu et al. 2023), as

$$v_{\text{rot}} = \frac{W_{20}}{2 \sin i}, \quad (15)$$

where i is the inclination angle. W_{20} employed in equation (15) has been corrected for instrumental broadening and redshift (Guo et al. 2020; Kent et al. 2008). In equation (15), we assume an alignment between the inclination angles of the stellar disk and HI disk, and then use the inclination angle of the stellar disk to estimate the inclination angle i of the HI disk (e.g. Guo et al. 2020; Hu et al. 2023; Du et al. 2019; Begum et al. 2008),

$$\sin i = \sqrt{\frac{1 - (b/a)^2}{1 - q_0^2}}, \quad (16)$$

where q_0 denotes the intrinsic axis ratio seen edge-on. We take $q_0 = 0.2$, which is commonly used in the previous studies (e.g. Du et al. 2019; Guo et al. 2020; Giovanelli et al. 1997; Tully et al. 2009). For those edge-on galaxies with g -band $b/a \leq 0.2$, we set $\sin i = 1$. Considering that the stellar disk and gas disk in galaxies may not be perfectly co-planar and often exhibit a small inclination difference of $\delta i < 20^\circ$ (e.g. Gault et al. 2021), we assume that the misalignment angle between the gas disk and the stellar disk, δi , follows a Gaussian distribution centred at 0° with a standard deviation of $\sigma = 20^\circ$. We treat σ as the error associated with i in our study.

4 RESULTS

For each LSBG, we thus obtain its g_{obs} and g_{bar} at the HI radius. g_{obs} as a function of g_{bar} for all of the sample LSBGs is shown in Fig. 1 (the upper panel), as depicted by the green points. We subsequently divide $\log(g_{\text{bar}})$ into different bins, and calculate the median $\log(g_{\text{obs}})$ of LSBGs in each bin. We find that the median values (depicted by the blue points) roughly follow the RAR of typical late-type galaxies given by McGaugh et al. (2016). We also directly employ the RAR equation,

$$g_{\text{obs}} = \frac{g_{\text{bar}}}{1 - e^{-\sqrt{g_{\text{bar}}/g_{\dagger}}}}, \quad (17)$$

to fit¹ the $g_{\text{obs}}\text{-}g_{\text{bar}}$ relation of our LSBG sample, and obtain the value of the free parameter g_{\dagger} . Our best-fitting result gives $g_{\dagger,\text{LSBG}} \simeq (1.71 \pm 0.13 \pm 0.16) \times 10^{-10} \text{ ms}^{-2}$. The RAR of our sample LSBGs

¹ using the *Python* orthogonal distance regression algorithm (scipy.odr)

coincides with the RAR of typical spiral galaxies and dwarf galaxies (Lelli et al. 2017; McGaugh et al. 2016) in the range of $\log(g_{\text{bar}}) \in [-12, -11]$, with an average difference of $\log(g_{\text{obs}})$ being merely 0.074 dex. This result indicates that, despite a large dispersion in the $g_{\text{obs}}\text{-}g_{\text{bar}}$ diagram, LSBGs exhibit mass distributions similar to those of typical late-type galaxies and dwarf galaxies in statistics.

For comparison, we also present the results of our control sample, i.e., HSBGs, in Fig. 1 (depicted by the grey points). We observe that, similar to the findings for typical late-type galaxies investigated by McGaugh et al. (2016), our HSBGs undeniably adhere to the universal RAR with a g_{\dagger} of $(1.57 \pm 0.11 \pm 0.12) \times 10^{-10} \text{ ms}^{-2}$. This adherence also suggests the robustness of our estimation of g_{bar} and g_{obs} .

5 SUMMARY AND DISCUSSION

Taking advantage of the ALFALFA HI survey data, we have selected the HI-rich LSBGs and estimated their gravitational accelerations g_{bar} and g_{obs} at the I radii. We find that, in statistics, LSBGs also conform to the universal RAR found in typical late-type galaxies as well as typical dwarf galaxies. Our results indicate that the distributions of dark matter and baryonic matter may still correlate with each other in LSBGs and that the mass distributions of the majority of LSBGs may be similar to those of ordinary late-type galaxies and dwarf galaxies. More specifically, our results suggest that the majority of LSBGs may have dark matter halos with masses and density profiles similar to typical late-type massive galaxies and dwarf galaxies.

Our investigation into the distribution of matter in LSBGs yields valuable insights into their formation mechanisms, offering a means to test and refine existing models of LSBG formation. Previous studies (e.g. McGaugh 1992; Dekel & Silk 1986) postulated that the low surface brightness of disk galaxies may stem from their formation within dark matter halos characterized by lower densities; however, this hypothesis would anticipate substantial deviations from the RAR for typical late-type galaxies. As such, our results suggest that this model may not fully encapsulate the formation and evolutionary processes of LSBGs.

Alternative theories suggest that LSBGs may originate from high-spin dark matter halos (e.g. Kim & Lee 2013; Mo et al. 1998), or may be influenced by feedback processes (Ludlow et al. 2017). While high spins of halos or feedback mechanisms may indeed lead to more extensive stellar distributions in galaxies, the correlated distributions of dark matter and baryonic matter profiles should not significantly deviate from the RAR observed in typical late-type galaxies. Therefore, our findings lend support to these two models of LSBG formation.

In this study, we have modelled the stellar and gaseous components of the LSBGs by two standard thin disks. We also consider a model in which both the gas and stars are uniformly distributed in spheres, respectively, and the results are shown in the lower panel of Fig. 1. We find that the RAR of both LSBGs and HSBGs do not change significantly with the different modelling. The same fitting method yields $g_{\dagger,\text{LSBG}} = (1.71 \pm 0.13 \pm 0.16) \times 10^{-10} \text{ ms}^{-2}$ and $g_{\dagger,\text{HSBG}} = (1.60 \pm 0.11 \pm 0.12) \times 10^{-10} \text{ ms}^{-2}$. Therefore, we conclude that the modelling method of baryonic matter distribution only has a minor effect on our results.

ACKNOWLEDGEMENTS

Y.R. acknowledges supports from the NSFC grant 12273037, and the CAS Pioneer Hundred Talents Program (Category B), as well

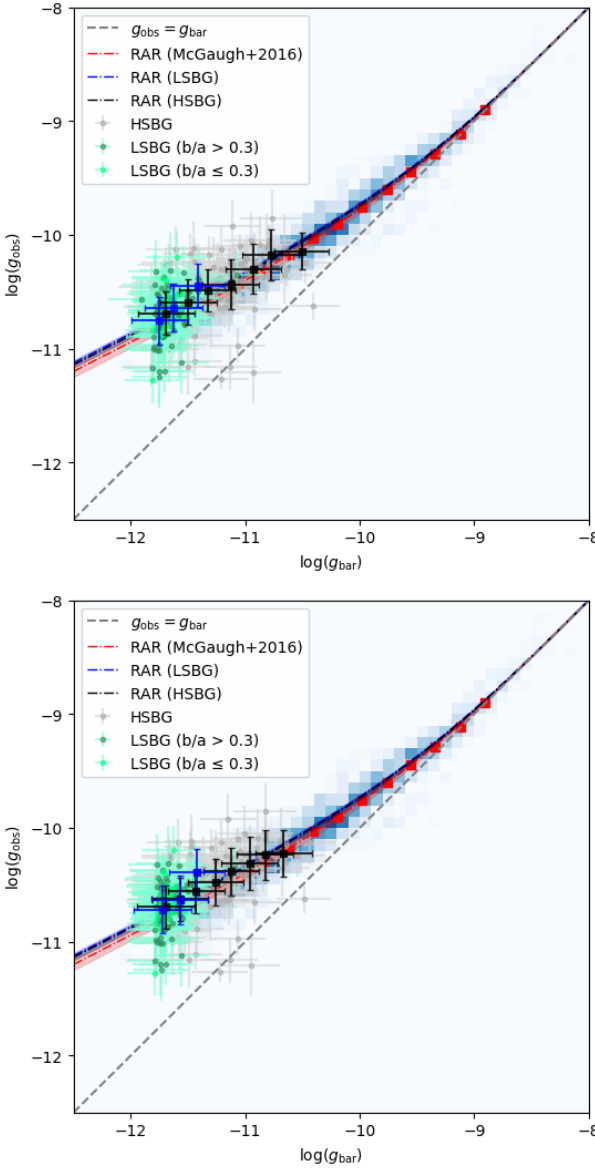


Figure 1. $g_{\text{bar}} - g_{\text{obs}}$ relationship of each sample, where we show LSBGs and the control sample (grey dots), as well as local spiral galaxies obtained by Lelli et al. (2017) using SPARC data (Lelli et al. 2016a). All the error bars represent 1σ deviations. Blue boxes are the results of LSBG binning, while black boxes are the results of control sample binning. Red boxes are bins in Lelli et al. (2017). The blue-dot-dashed line and black-dot-dashed line are the fitted lines by our LSBG sample and HSBG sample, respectively, and the red-dot-dashed line is the universal RAR by Lelli et al. (2017). The shaded area around a curve with the same colour represents the 1σ deviation of g_{bar} of this curve. The grey-dashed line is the identical line. The upper panel: stars and gas are assumed to be distributed in standard thin disks, respectively. The lower panel: stars and gas are assumed to distribute in uniform spheres, respectively.

as the USTC Research Funds of the Double First-Class Initiative (No. YD2030002013). H.H. is supported by the Fundamental Research Funds for the Central Universities, the CAS Project for Young Scientists in Basic Research Grant No. YSBR-062, the National SKA Program of China No. 2022SKA0110201, and the NSFC grant No. 12033008.

DATA AVAILABILITY

Data are available if requested.

REFERENCES

Amorisco N. C., Loeb A., 2016, *MNRAS*, **459**, L51
 Begum A., Chengalur J. N., Karachentsev I. D., Sharina M. E., 2008, *MNRAS*, **386**, 138
 Behroozi P. S., Wechsler R. H., Conroy C., 2013, *ApJ*, **770**, 57
 Bothun G., Impey C., McGaugh S., 1997, *PASP*, **109**, 745
 Broeils A. H., Rhee M. H., 1997, *A&A*, **324**, 877
 Carleton T., Errani R., Cooper M., Kaplinghat M., Peñarrubia J., Guo Y., 2019, *MNRAS*, **485**, 382
 Chae K.-H., Bernardi M., Domínguez Sánchez H., Sheth R. K., 2020, *ApJ*, **903**, L31
 Chan T. K., Kereš D., Wetzel A., Hopkins P. F., Faucher-Giguère C. A., El-Badry K., Garrison-Kimmel S., Boylan-Kolchin M., 2018, *MNRAS*, **478**, 906
 Dekel A., Silk J., 1986, *ApJ*, **303**, 39
 Du W., Wu H., Lam M. I., Zhu Y., Lei F., Zhou Z., 2015, *AJ*, **149**, 199
 Du W., Cheng C., Wu H., Zhu M., Wang Y., 2019, *MNRAS*, **483**, 1754
 Durbala A., Finn R. A., Crone Odekon M., Haynes M. P., Koopmann R. A., O'Donoghue A. A., 2020, *AJ*, **160**, 271
 El-Badry K., et al., 2018, *MNRAS*, **477**, 1536
 Freeman K. C., 1970, *ApJ*, **160**, 811
 Gault L., et al., 2021, *ApJ*, **909**, 19
 Giovanelli R., Haynes M. P., Herter T., Vogt N. P., Wegner G., Salzer J. J., da Costa L. N., Freudling W., 1997, *AJ*, **113**, 22
 Grudić M. Y., Boylan-Kolchin M., Faucher-Giguère C.-A., Hopkins P. F., 2020, *MNRAS*, **496**, L127
 Guo Q., et al., 2020, *Nature Astronomy*, **4**, 246
 Haynes M. P., et al., 2011, *AJ*, **142**, 170
 He M., Wu H., Du W., Liu H.-y., Lei F.-j., Zhao P.-s., Zhang B.-q., 2020, *ApJS*, **248**, 33
 Hu H.-J., Guo Q., Zheng Z., Yang H., Tsai C.-W., Zhang H.-X., Zhang Z.-Y., 2023, *ApJ*, **947**, L9
 Impey C., Bothun G., 1997, *ARA&A*, **35**, 267
 Keller B. W., Wadsley J. W., 2017, *ApJ*, **835**, L17
 Kent B. R., et al., 2008, *AJ*, **136**, 713
 Kim J.-h., Lee J., 2013, *MNRAS*, **432**, 1701
 Kravtsov A. V., Vikhlinin A. A., Meshcheryakov A. V., 2018, *Astronomy Letters*, **44**, 8
 Kuzio de Naray R., McGaugh S. S., de Blok W. J. G., 2004, *MNRAS*, **355**, 887
 Leisman L., et al., 2017, *ApJ*, **842**, 133
 Lelli F., McGaugh S. S., Schombert J. M., 2016a, *AJ*, **152**, 157
 Lelli F., McGaugh S. S., Schombert J. M., 2016b, *ApJ*, **816**, L14
 Lelli F., McGaugh S. S., Schombert J. M., Pawlowski M. S., 2017, *ApJ*, **836**, 152
 Li P., Lelli F., McGaugh S., Schombert J., 2018, *A&A*, **615**, A3
 Li P., McGaugh S. S., Lelli F., Tian Y., Schombert J. M., Ko C.-M., 2022, *ApJ*, **927**, 198
 Ludlow A. D., et al., 2017, *Phys. Rev. Lett.*, **118**, 161103
 Mancera Piña P. E., et al., 2019, *ApJ*, **883**, L33
 McGaugh S. S., 1992, PhD thesis, University of Michigan
 McGaugh S. S., 2012, *AJ*, **143**, 40
 McGaugh S. S., Schombert J. M., 2015, *ApJ*, **802**, 18
 McGaugh S. S., Schombert J. M., Bothun G. D., de Blok W. J. G., 2000, *ApJ*, **533**, L99
 McGaugh S. S., Lelli F., Schombert J. M., 2016, *Phys. Rev. Lett.*, **117**, 201101
 Mo H. J., McGaugh S. S., Bothun G. D., 1994, *MNRAS*, **267**, 129
 Mo H. J., Mao S., White S. D. M., 1998, *MNRAS*, **295**, 319
 Mowla L., van Dokkum P., Merritt A., Abraham R., Yagi M., Koda J., 2017, *ApJ*, **851**, 27
 Navarro J. F., Benítez-Llambay A., Fattahi A., Frenk C. S., Ludlow A. D., Oman K. A., Schaller M., Theuns T., 2017, *MNRAS*, **471**, 1841

Noguchi M., 2001, [MNRAS](#), **328**, 353

Papastergis E., Adams E. A. K., van der Hulst J. M., 2016, [A&A](#), **593**, A39

Paranjape A., Sheth R. K., 2021, [MNRAS](#), **507**, 632

Pérez-Montaña L. E., Cervantes Sodi B., 2019, [MNRAS](#), **490**, 3772

Prole D. J., et al., 2019, [MNRAS](#), **484**, 4865

Richards E. E., et al., 2018, [MNRAS](#), **476**, 5127

Rong Y., Guo Q., Gao L., Liao S., Xie L., Puzia T. H., Sun S., Pan J., 2017, [MNRAS](#), **470**, 4231

Rong Y., Li H., Wang J., et al. 2018, [MNRAS](#), **477**, 230

Rong Y., Dong X.-Y., Puzia T. H., et al. 2020a, [ApJ](#), **899**, 78

Rong Y., Zhu K., Johnston E. J., Zhang H.-X., Cao T., Puzia T. H., Galaz G., 2020b, [ApJ](#), **899**, L12

Saburova A. S., Chilingarian I. V., Katkov I. Y., Egorov O. V., Kasparova A. V., Khoperskov S. A., Uklein R. I., Vozyakova O. V., 2018, [MNRAS](#), **481**, 3534

Saburova A. S., Chilingarian I. V., Kasparova A. V., Sil'chenko O. K., Grishin K. A., Katkov I. Y., Uklein R. I., 2021, [MNRAS](#), **503**, 830

Tully R. B., Rizzi L., Shaya E. J., Courtois H. M., Makarov D. I., Jacobs B. A., 2009, [AJ](#), **138**, 323

Verheijen M. A. W., 1997, PhD thesis, Univ. Groningen

Wang J., Koribalski B. S., Serra P., van der Hulst T., Roychowdhury S., Kamphuis P., Chengalur J. N., 2016, [MNRAS](#), **460**, 2143

Wheeler C., Hopkins P. F., Doré O., 2019, [ApJ](#), **882**, 46

Wright A. C., Tremmel M., Brooks A. M., Munshi F., Nagai D., Sharma R. S., Quinn T. R., 2021, [MNRAS](#), **502**, 5370

Wyder T. K., et al., 2009, [ApJ](#), **696**, 1834

Zhu Q., Pérez-Montaña L. E., Rodriguez-Gomez V., Cervantes Sodi B., Zjupa J., Marinacci F., Vogelsberger M., Hernquist L., 2023, [MNRAS](#), **523**, 3991

de Blok W. J. G., McGaugh S. S., 1997, [MNRAS](#), **290**, 533

van Dokkum P. G., Abraham R., Merritt A., Zhang J., Geha M., Conroy C., 2015a, [ApJ](#), **798**, L45

van Dokkum P. G., et al., 2015b, [ApJ](#), **804**, L26

van Dokkum P., et al., 2018, [Nature](#), **555**, 629

This paper has been typeset from a \TeX / \LaTeX file prepared by the author.